

Chapter 1

Model Reduction for Transport-Dominated Problems via Cross-Correlation Based Snapshot Registration

Harshith Gowrachari^[0009-0001-0527-9632],
Giovanni Stabile^[0000-0003-3434-8446],
Gianluigi Rozza^[0000-0002-0810-8812].

Abstract :

Traditional linear approximation methods, such as proper orthogonal decomposition and the reduced basis method, are ineffective for transport-dominated problems due to the slow decay of the Kolmogorov n -width. This results in reduced-order models that are both inefficient and inaccurate. In this work, we present an approach for the model reduction of transport-dominated problems by employing cross-correlation based snapshot registration, accelerating the Kolmogorov n -width decay, and enabling the construction of efficient reduced-order models using linear methods. We propose a complete framework comprising offline-online stages for the development of reduced-order models using the cross-correlation based snapshots registration. The effectiveness of the proposed approach is demonstrated using two test cases: 1D travelling waves and the higher-order methods benchmark test case, 2D isentropic convective vortex.

1.1 Introduction

Reduced order modelling has become a rapidly advancing field in computational science and engineering. Industries have a keen interest in obtaining reduced-order models (ROMs) for engineering systems, particularly in applications involving con-

Harshith Gowrachari
Mathematics Area, mathLab, International School for Advanced Studies, via Bonomea 265, 34136 Trieste, Italy. e-mail: hgowrach@sissa.it

Giovanni Stabile
Biorobotics Institute, Sant'Anna School of Advanced Studies, V.le R. Piaggio 34, 56025, Pontedera, Pisa, Italy. e-mail: giovanni.stabile@santannapisa.it

Gianluigi Rozza
Mathematics Area, mathLab, International School for Advanced Studies, via Bonomea 265, 34136 Trieste, Italy. e-mail: grozza@sissa.it

trol, optimization, and uncertainty quantification. They offer significant computational efficiency in many query scenarios and are suitable for real-time computations. These models achieve computational efficiency by approximating high-dimensional parametric partial differential equations (PDEs) with low-dimensional representations, substantially reducing the numerical simulation cost compared to full-order models (FOMs).

Numerical methods such as the finite element method (FEM), finite volume method (FVM), discontinuous Galerkin method (DGM), and spectral element method (SEM) are widely used to solve parametric PDEs describing real-world scenarios. Although these methods ensure accuracy, they come with high computational costs. The reduced order modelling (ROM) framework tackles this in two stages: 1) Offline (training) stage – This computationally expensive phase involves calculating a series of FOM solutions (snapshots) and constructing the ROM by approximating the FOM solution manifold with a low-dimensional reduced subspace. 2) Online (testing and predictive) stage: This computationally efficient phase leverages the compressed data obtained during the offline stage to predict reduced solutions for new, unseen parameters, significantly reducing computational expenses.

Several model reduction techniques are available to derive low-dimensional approximation subspaces [31, 16, 6, 34]. Among these, linear approximation methods like proper orthogonal decomposition (POD) and reduced basis (RB) methods are widely used and highly effective in various applications. However, certain problems of interest, such as transport-dominated problems, exhibit slow decay of Kolmogorov n -width. This slow decay limits the model reduction achievable through linear subspace approximations [30].

The solution manifolds of the transport-dominated problems, such as travelling waves, convective vortex, and vortex shredding often exhibit slow decay of the Kolmogorov n -width (KnW), making it difficult to obtain a low-dimensional linear approximation subspace for the construction of accurate and efficient reduced-order models (ROMs). The KnW, as defined in [30], provides a rigorous measure of the reducibility of the solution manifold \mathcal{M} using linear approximation subspaces.

For a solution manifold \mathcal{M} comprising f elements (solutions across all time instances) embedded in a normed linear space $(X_N, \|\cdot\|_{X_N})$, the Kolmogorov n -width $d_n(\mathcal{M})$ is defined as:

$$d_n(\mathcal{M}) := \inf_{E_n \subset X_N} \sup_{f \in \mathcal{M}_N} \inf_{g \in E_n} \|f - g\|_{X_N} \quad (1.1)$$

where E_n is a linear subspace of X_N with dimension n . The KnW $d_n(\mathcal{M})$ represents the maximum approximation error obtained when any element $f \in \mathcal{M}$ is approximated by an element $g \in E_n$. Additionally, as faster the $d_n(\mathcal{M})$ decay with increasing n indicates how effectively a low-dimensional linear subspace of dimen-

sion n can approximate the solution manifold \mathcal{M} .

Recent advancements in model-reduction techniques have focused on addressing the challenges posed by slow Kolmogorov n -width decay, the main reason for the development of non-linear approaches [28]. These methods include performing model reduction on non-linear manifolds, such as obtaining non-linear trial subspaces using convolutional autoencoders (CAEs) [20, 15, 7, 17, 22, 11, 21, 33], and applying quadratic approximation manifolds [19, 1, 12]. Other strategies involve incorporating adaptive enrichment techniques, [14, 44, 29, 27, 3], and transforming linear subspaces through transport maps using registration methods [26, 23, 18, 24, 4, 32, 40, 42, 25]. The registration methods yield the low-dimensional transformed linear subspace that is effective in approximating the full-order solutions.

In this work, we apply cross-correlation-based snapshot registration for model reduction of transport-dominated problems. This method uses cross-correlation to align multiple snapshots to a reference, accelerating the decay of KnW and yielding a low-dimensional approximation subspace for efficient ROM construction. It is particularly effective for problems where traditional linear methods suffer, offering a more robust way to capture the essential behaviour of the system and enabling the development of accurate, reduced-order models using the transformed (registered) linear approximation subspace.

In reduced-order modelling, once the reduced approximation subspace is obtained, it is necessary to compute the evolution of the dynamics within this reduced subspace. This requires determining modal coefficients or latent coordinates, which can be achieved using either intrusive or non-intrusive methods. In the intrusive approach, the discretized governing equations (PDEs) are projected onto the low-dimensional subspace, leading to a system of low-dimensional ODEs. This process, known as Galerkin or Petrov-Galerkin projection-based ROM, is discussed in [37, 38]. In this work, we focus specifically on non-intrusive methods, where, after obtaining the set of snapshots, the ROM is constructed using proper orthogonal decomposition (POD) with regression (POD-R) and we discuss this method in the following section.

This article is organized as follows, in section 1.2 we discuss the construction of a non-intrusive or data-driven reduced order model using POD with regression (POD-R) strategy; in section 1.3 we discuss the employment of the cross-correlations base snapshots registration approach; in section 1.4 the implementation of the complete algorithm for the development of ROM utilizing the cross-correlations base registration is mentioned; in section 1.5 we test our proposed approach by applying to transport-dominated problems, 1D travelling waves and 2D isentropic convective vortex; and in section 1.6 the conclusions, perspectives, and future directions are discussed.

1.2 Reduced-order modelling of time-dependent problems

Given that we are focusing on time-dependent problems, we consider the abstract partial differential equation (PDE) problem described in (1.2), defined over the domain $\Omega \subset \mathbb{R}^n$ and the time interval $T = [0, t_f]$:

$$\mathcal{L}(s(t)) = 0, \quad t \in T \quad (1.2)$$

Where $s(t)$ is an unknown function, the operator \mathcal{L} incorporates the differential operators, forcing terms and boundary conditions that govern the dynamics of $s(t)$. To obtain the full-order solutions of the given time-dependent problem, here we consider the finite-difference method, but one can choose to use any numerical method such as the finite-volume method or finite-element method. We denote the solutions database as a set of time-snapshot pairs given by $\{t_i, s_i\}_{i=1}^{N_T}$ with $t_i \in T \subset \mathbb{R}^{N_T}$ with N_T number of time instances and $s_i \in \mathbb{R}^{N_h}$ with N_h number of degrees of freedom. We represent the snapshots matrix $S \in \mathbb{R}^{N_h \times N_T}$ as :

$$S = \begin{bmatrix} | & | & & | \\ s_1 & s_2 & \dots & s_{N_T} \\ | & | & & | \end{bmatrix}. \quad (1.3)$$

To reduce the computational cost of the associated discretization method, in this section, we present the framework for non-intrusive ROMs using proper orthogonal decomposition (POD) with regression (POD-R) [41]. Here, we first recall the POD, a widely used linear approximation method in ROMs, and is exploited together with the regression strategy to obtain efficient ROMs.

1.2.1 Proper orthogonal decomposition

We use POD to obtain the reduced linear approximation subspace U_r , where $\dim(U_r) = N_r \ll N_h$, which consists of POD modes column-wise. The POD modes are computed by using the singular value decomposition (SVD) [39] of the snapshots matrix:

$$S = U \Sigma V^T, \quad (1.4)$$

where, where, $U \in \mathbb{R}^{N_h \times N_h}$ and $V \in \mathbb{R}^{N_T \times N_T}$ are the two orthonormal matrices. $\Sigma \in \mathbb{R}^{N_h \times N_T}$ is the diagonal matrix with r non-zero singular values, arranged in descending order $\sigma_1 \geq \sigma_2 \geq \dots \geq \sigma_r > 0$, which indicates the energy contribution of the corresponding modes. Here, r is the rank of the snapshot matrix S . The reduced linear approximation subspace $U_r \in \mathbb{R}^{N_h \times N_r}$ is constructed such that :

$$\mathbf{U}_r = \underset{\mathbf{U} \in \mathbb{R}^{N_h \times N_r}}{\operatorname{argmin}} \frac{1}{\sqrt{N_T}} \|\mathbf{S} - \hat{\mathbf{U}} \hat{\mathbf{U}}^T \mathbf{S}\|_F, \quad (1.5)$$

where $\|\cdot\|_F$ is a frobenius norm and S is the snapshots matrix.

The POD modes are column entries of the left singular matrix U corresponding to the largest singular values. The energy retained by the first m modes is given by the ratio of the energy contained by the first m modes and the energy contained by all r modes :

$$E(m) = \frac{\sum_{i=1}^m \sigma_i^2}{\sum_{i=1}^r \sigma_i^2}. \quad (1.6)$$

Generally, the reduced space U_r is constructed by considering the first N_r columns of U [10], such that the $E(N_r)$ contains a user-defined threshold, usually about 95 – 99.9% of the total eigenvalue energy.

1.2.2 POD with regression (POD-R)

The proper orthogonal decomposition with regression strategy is employed to obtain non-intrusive data-driven ROM [41], which exploits regression to approximate the trajectories of the full-order model. Once we have the reduced space U_r , we approximate the solutions of $s(t)$ by reduced expansion:

$$s(t) = U_r c_r(t) \quad (1.7)$$

where, $c_r \in \mathbb{R}^{N_r}$ is the temporal expansion coefficients. We compute the temporal expansion coefficients as shown in (1.8), by projecting the snapshot matrix S onto the reduced subspace U_r .

$$c(t_i) = U_r^T s(t_i) \quad \forall i = 1, \dots, N_{train}. \quad (1.8)$$

We can only approximate the snapshots of the initial database (training set) via these temporal expansion coefficients. To predict snapshots for new time instances, we need to build a map from time t_i to c_i temporal expansion coefficients. Here, the main aim is to construct a regression $\mathcal{I} : T \mapsto \mathbb{R}^{N_r}$ which approximates the map \mathcal{F} as in (1.9) given by a set of N_{train} input-output pairs $\{t_i, c_i\}_{i=1}^{N_{train}}$, where t_i is the time associated with the i^{th} snapshot and c_i are the corresponding temporal coefficients obtained by (1.8).

$$\mathcal{F} : t \in T \mapsto c \in \mathbb{R}^{N_r}. \quad (1.9)$$

To construct this regression \mathcal{I} , there are various techniques available, such as linear interpolation, Gaussian process regression (GPR), radial basis function (RBF) interpolation, multi-fidelity methods, and artificial neural networks (ANNs), to name few. In this work, we exploit radial basis function (RBF) interpolation to devise this map. The constructed regression model is used to predict the snapshot s^* for new

time instance t^* via inverse coordinate transformation:

$$\mathbf{s}(t^*) = U_r I(t^*). \quad (1.10)$$

1.3 Cross-correlation based snapshot registration

Cross-correlation measures the similarity between two signals as a function of the time shift or lag between them. It plays a crucial role in signal processing, pattern recognition, time series analysis, and filtering. Cross-correlation aids in identifying or quantifying the relationships between signals and is used to detect signals that are embedded in noise. Image registration through cross-correlation is an essential and widely adopted technique in the field of medical imaging [2, 5]. In this work, we exploit cross-correlation to register the snapshots of transport-dominated problems and aim to accelerate the KnW decay.

Continuous cross-correlation: Let us consider two continuous-time signals $f(t)$ and $g(t)$, where $t \in \mathbb{R}$ is the continuous-time variable. The continuous cross-correlation $R_{fg}(\Delta t)$ between $f(t)$ and $g(t)$ at a time lag $\Delta t \in \mathbb{R}$ is defined as:

$$R_{fg}(\Delta t) = \int_{-\infty}^{\infty} f(t) \cdot g(t + \Delta t) dt \quad (1.11)$$

where, $f(t)$ is a signal at time t and $g(t + \Delta t)$ is a signal at time $t + \Delta t$, which represents the time shift of Δt relative to $f(t)$. By definition, the continuous cross-correlation is computed by integrating the product of $f(t)$ and $g(t + \Delta t)$ over the entire time domain, from $-\infty$ to $+\infty$.

Discrete cross-correlation: Let us consider two discrete-time signals $f[t]$ and $g[t]$, where $t \in \mathbb{R}$ is the discrete time. The discrete cross-correlation $R_{fg}(\Delta t)$ between the signals $f[t]$ and $g[t]$ at a time lag Δt is defined as:

$$R_{fg}[\Delta t] = \sum_t f[t] \cdot g[t + \Delta t] \quad (1.12)$$

where, $f[t]$ is the signal at time t and $g[t + \Delta t]$ is the signal at time $t + \Delta t$, representing a time shift of Δt relative to $f[t]$. The discrete cross-correlation is computed by performing a summation of the product of $f[t]$ and $g[t + \Delta t]$ overall the values of t .

Cross-correlation provides a robust framework for analyzing the relationship between time-shifted signals. In this work, we exploit cross-correlation to employ the registration of snapshots, addressed in Algorithm 1. The cross-correlation between each snapshot s_i and the reference snapshot s^{ref} is used to compute the shifts that employ registration. Here, we employ the registration of snapshots via cross-correlation to circumvent KnW decay for transport-dominated problems. This method aims to

find the optimal shift for each snapshot, aligning the snapshots to the reference, based on the maximization of their cross-correlation.

The process of cross-correlations based registration is as follows: At first, we choose a set of training snapshots $\{s_1, s_2, \dots, s_{N_{train}}\}$ for corresponding time instances $\{t_1, t_2, \dots, t_{N_{train}}\}$ and one among them a reference snapshot s^{ref} . For each training snapshot s_i , we compute the cross-correlation¹ between the reference s^{ref} and the s_i at different time shifts (time-steps) Δt . Cross-correlation measures the similarity between two signals as a function of their relative time displacement. The optimal shift Δ_i for each snapshot s_i is determined by finding the index of maximum correlation, i.e., the shift that produces the highest similarity between the reference snapshot and the respective snapshot. This is computed by finding the index Δ_i where the cross-correlation is maximized. Once the optimal time shift Δ_i is found for each snapshot s_i , we apply these shifts to the snapshot to align with the reference s^{ref} . Now, all the snapshots are aligned with the reference snapshot and we store registered snapshots s_i^{ref} and the optimal shifts for subsequent steps in developing the ROM.

Algorithm 1 : Registration via cross-correlation

- 1: **Input**: Set of training snapshots $\{s_1, s_2, \dots, s_{N_{train}}\}$ for corresponding time instances $\{t_1, t_2, \dots, t_{N_{train}}\}$, reference snapshot s^{ref}
- 2: **Output**: Set of Registered snapshots $\{s_1^{ref}, s_2^{ref}, \dots, s_{N_{train}}^{ref}\}$, corresponding shifts $\Delta = \{\Delta_1, \Delta_2, \dots, \Delta_{N_{train}}\}$
- 3: **for** each snapshot s_i in training snapshots **do**
- 4: Calculate the cross-correlation between the reference snapshot r and the snapshot s_i :

$$\text{correlation}(r, s_i) = \text{correlate}(r, s_i)$$

- 5: Calculate the optimal shift Δ_i as:

$$\Delta_i = \text{argmax}(\text{correlation}(r, s_i)) - (N_h - 1)$$

- 6: Apply the shift Δ_i to the snapshot s_i using circular shift:

$$s_i^{ref} = \text{shift}(s_i, \Delta_i)$$

- 7: Store the Registered snapshot s_i^{ref} and the shift Δ_i
 - 8: **end for**
 - 9: **return** the set of Registered snapshots $S^{ref} = \{s_1^{ref}, s_2^{ref}, \dots, s_{N_{train}}^{ref}\}$ and shifts Δ_i .
-

¹ We use `scipy` python library to compute correlation

1.4 ROM via cross-correlation based snapshot registration

In this section, we discuss the complete workflow for constructing ROMs using a cross-correlation based snapshot registration approach. As reported in Algorithm 2, the complete workflow is divided into two phases, the offline phase in which registration of snapshots and ROM is constructed, and in the offline phase, the ROM predictions which are at the reference are reverted to the correct physical frame.

In the offline phase, the time-snapshots pairs $\{t_i, s_i\}_{i=1}^{N_{train}}$, the snapshots are registered using the Algorithm 1, which exploits cross-correlation to employ registration and results in a registered snapshots matrix S^{ref} and a corresponding shift matrix Δ . Now, all the snapshots are in the same physical reference frame, accelerating the KnW and yielding the low-dimension linear approximation subspace. We construct ROM ² on the registered snapshots matrix S^{ref} , following the steps mentioned in section 1.2 and we use RBF for the regression in this task. Here, to obtain shifts for new time instances in the online phase, we build map α using regression for $\{t_i, \Delta_i\}$ pairs. In the online phase, the ROM predictions are at the reference where the ROM is constructed. We exploit the predicted optimal shifts obtained by the map α , to revert the snapshots to the correct physical frame.

Algorithm 2 : ROM via cross-correlation based snapshot registration

- 1: **Input:** Set of training snapshots $\{s_1, s_2, \dots, s_{N_{train}}\}$ for corresponding time instances $\{t_1, t_2, \dots, t_{N_{train}}\}$, reference snapshot s^{ref} , N_r number of POD modes.
- 2: **Output:** Prediction of snapshots via cross-correlation based snapshots registration.

Offline phase - Training stage

- 3: Registration of snapshots via cross-correlation using Algorithm 1:
Obtain the Registered snapshots matrix S^{ref} and the corresponding optimal shifts matrix Δ
- 4: Construct ROM on the registered snapshots matrix S^{ref} following the steps in section 1.2.

$$rom = ROM(S^{ref}, POD, RBF)$$

- 5: Construct map α using regression for $\{t_i, \Delta_i\}$ pairs: To predict shifts for new time instances in the online phase.

Online phase - Testing and prediction stage

- 6: **for** each new time instance t_i in test set: **do**
- 7: $s_i^{ref} = rom.predict(t_i)$
- 8: Obtain the optimal shift Δ_i^* using map α .
- 9: Transport back the predicted snapshots to the correct frame by reverting it with the optimal shift:

$$s_i = shift(s_i^{ref}, -\Delta_i^*)$$

- 10: **end for**
 - 11: **return** the set of predicted snapshots $\{s_1, s_2, \dots, s_{N_{test}}\}$ in correct physical frame.
-

² using EZyRB package [9], a Python library for data-driven ROMs.

1.5 Numerical experiments

In this section, we evaluate the proposed approach to model reduction using cross-correlation-based snapshot registration to construct ROMs for transport-dominated problems. We consider two numerical experiments: the 1D travelling waves and a higher-order benchmark test case - the 2D isentropic convective vortex.

1.5.1 1D Travelling wave

We consider a parameterized 1D Gaussian function (1.13) to mimic the solutions of the linear transport equation considered in [11, 12], with $\alpha = 1$, $x \in [0, 10.25]$ is the spatial coordinate, constant σ (standard deviation), and $t \in [0, 10.25]$ is the mean, interpreted here as time to treat this as a parameterized time-dependent problem. We generate a database consisting of 100-time instances and their corresponding snapshots over the 256 equidistant spatial nodes in $x \in [0, 10.25]$. We divide 50% of the database as a training set and the rest as a testing set, as shown in the Figure (1.1)

$$f(t) = \alpha e^{-(x-t)^2/(2\sigma^2)}. \quad (1.13)$$

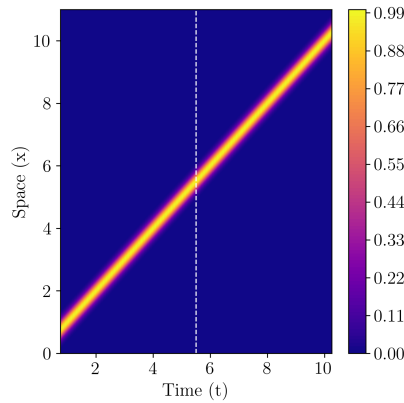


Fig. 1.1: 2D contour of the original snapshots of the 1D travelling waves. Here, the white line separates the first 50% dataset as the training set and the rest as the test set.

In the offline phase, we select the reference snapshot corresponding to the parameter $t = 3.03$. Using the procedure outlined in Algorithm 1, we perform snapshots registration, aligning multiple snapshots to the reference by leveraging correlation-

based registration, as shown in Figure 1.2. From Figure 1.3 it is evident the registration has a significant effect on accelerating the KnW decay, meaning we can seek for low-dimensional reduced subspace for the construction of ROM. Figure 1.3b shows the first POD mode obtained by employing registration, which captures the structure of the Gaussian travelling waves. In the case of unregistered snapshots, we have to consider numerous POD modes to construct ROM, which leads to inefficient ROMs. We construct ROM by considering the first POD mode obtained via registration and we exploit the POD-R strategy discussed in section 1.2. Here, we utilize the radial basis function (RBF) interpolation for the regression task.

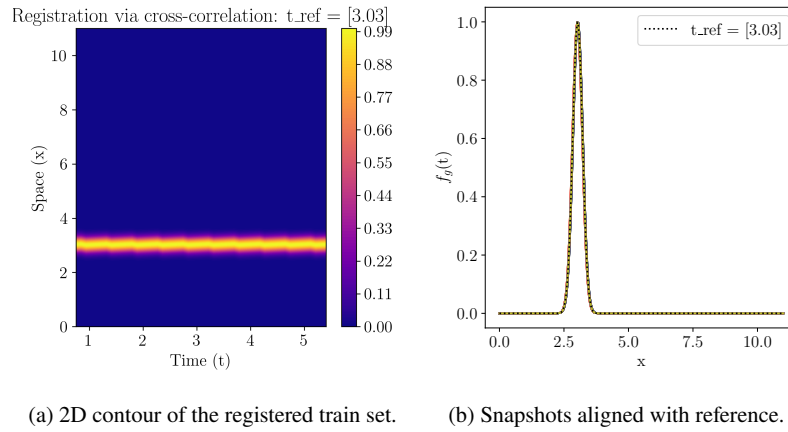


Fig. 1.2: 1D travelling waves training set registered at the reference configuration.

After constructing the ROM, we incorporate shifts in the online phase by creating parameter t_i -to-optimal- Δ_i mappings (denoted as α in Algorithm 2) using linear interpolation in this experiment. To predict snapshots at new time instances, we utilize the regression α to revert the ROM-predicted snapshots (at the reference frame) back to the correct physical frame. Figure 1.4 presents the predicted snapshots transformed to the correct physical frame for both training and testing, alongside the original snapshots as the ground truth and the absolute differences between the predictions and the truth. The relative prediction error is depicted in Figure 1.5, showing that the errors for both training and testing parameters are of the same order of magnitude, with the mean relative error highlighted.

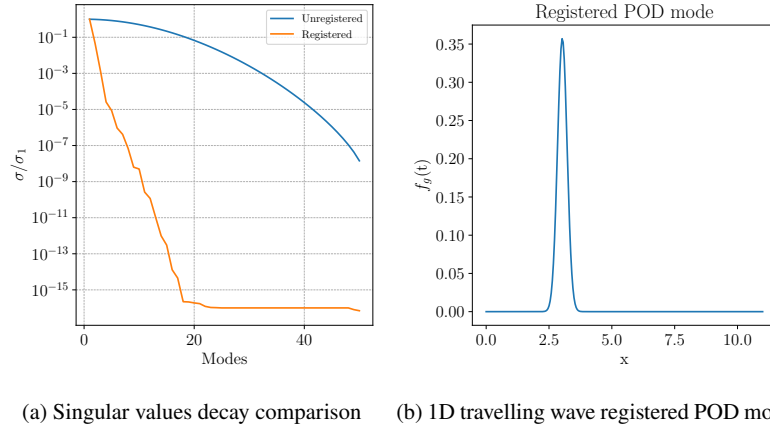


Fig. 1.3: **Left:** Comparison of the singular values of registered and unregistered 1D travelling waves, and **Right:** the first POD mode of the registered snapshots matrix

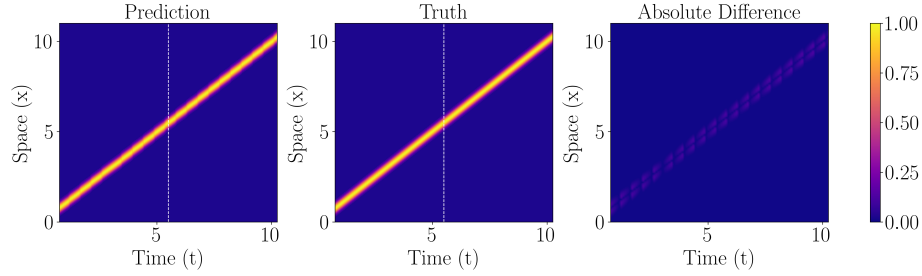


Fig. 1.4: Comparison of the predictions of the resulted ROM of the 1D travelling waves with the original snapshots as ground truth, here the white line separates the first 50% dataset as the training set and remaining as the test set and also showing the absolute difference between the prediction and the ground truth.

1.5.2 2D isentropic convective vortex

For the second experiment, we consider the 2D isentropic convective vortex, a popular higher-order method benchmark case [36, 43]. To describe the flow physics of the inviscid, compressible flow of our benchmark case, we consider the 2D Unsteady Euler equations:

$$\frac{\partial}{\partial t} \begin{bmatrix} \rho \\ \rho u \\ \rho v \\ E \end{bmatrix} + \frac{\partial}{\partial x} \begin{bmatrix} \rho u \\ \rho u^2 + p \\ \rho uv \\ u(E + p) \end{bmatrix} + \frac{\partial}{\partial y} \begin{bmatrix} \rho v \\ \rho uv \\ \rho v^2 + p \\ v(E + p) \end{bmatrix} = 0 \quad (1.14)$$

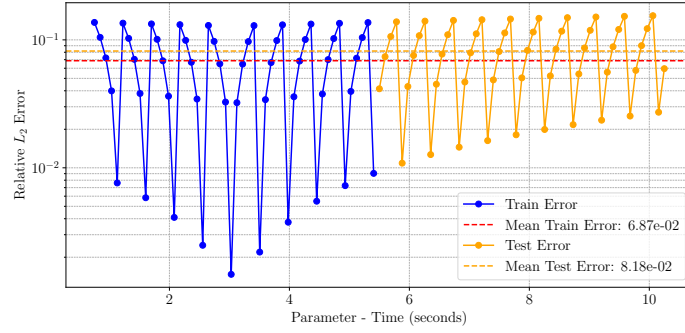


Fig. 1.5: Relative L_2 predictions error by the ROM of the 1D travelling wave via cross-correlation base snapshots registration, for both training set and test set parameters.

$$E = \frac{p}{\gamma - 1} + \frac{1}{2}\rho(u^2 + v^2). \quad (1.15)$$

Here, ρ is density, (u, v) are velocity x and y component, p is pressure and E is total energy. In this test case, we consider constant specific heat ratio, $\gamma = 1.4$, and gas constant, $R_{gas} = 287.15$ J/Kg.K. The thermodynamic closure is attained by the total energy equation (1.15).

$$\begin{cases} \rho = \left[1 - \frac{(\gamma-1)b^2}{8\gamma\pi^2} e^{1-r^2} \right]^{\frac{1}{\gamma-1}}, \\ p = \rho^\gamma, \\ u = u_\infty - \frac{b}{2\pi} e^{\frac{1}{2}(1-r^2)} (y - y_c), \\ v = v_\infty + \frac{b}{2\pi} e^{\frac{1}{2}(1-r^2)} (x - x_c). \end{cases} \quad (1.16)$$

The freestream flow is initialized with the conditions $\rho_\infty = 1$, $u_\infty = 0.1$, $v_\infty = 0$, and $p_\infty = 1$. The vortex is introduced into the domain based on the analytical solution described in (1.16), with a vortex strength of $b = 0.5$, a vortex radius $r = \sqrt{(x - x_c)^2 + (y - y_c)^2} = 0.5$, and a vortex centre located at $(x_c, y_c) = (5, 10)$. Several variations of the vortex problem have been reported in the literature [35]. In this study, we adopt the version implemented in the HyPar 1.0 package— finite difference hyperbolic-parabolic PDE solver on cartesian grids [8] and we use this package to obtain the full-order solution of the equation 1.14.

To approximate the spatial derivatives in the governing equations, we consider the fifth-order hybrid-compact weighted essentially non-oscillatory (WENO) scheme, a high-order accurate numerical method suitable for hyperbolic partial differential equations and convection-dominated problems [45]. For time integration, the third-

order strong stability-preserving Runge-Kutta (SSPRK3) method is utilized [13].

We consider the rectangular computational domain $\Omega = [0, 40] \times [0, 20]$ is discretized into 28,800 Cartesian grid points. To impose a vortex into the domain, we consider the initial conditions mentioned above. The simulation is conducted over the time interval $t \in [0, 62.5]$ using a time step of $\Delta t = 0.00625$, the snapshots are recorded every 100 time-steps Δt , resulting in a snapshot matrix containing density field snapshots at $N_T = 100$ time instances. The full-order solutions (snapshots) at three different time instances are shown in Figure 1.6.

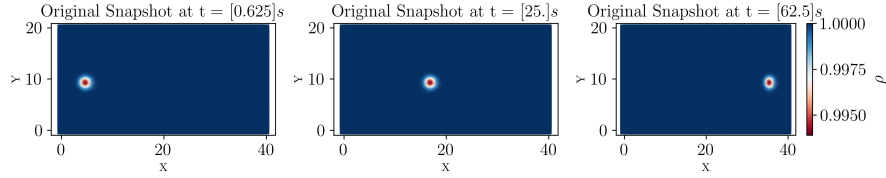


Fig. 1.6: Full-order solutions of the isentropic convective vortex at time instances, $t \in \{0.625, 25, 62.5\}$.

In this numerical experiment, we consider the first 30% dataset as a training set and the rest as the test set. We perform registration on the training set, Figure 1.7 shows the registered snapshots at time instances $t \in \{0.625, 25, 62.5\}$, comparing with the reference and the corresponding original snapshot. We perform reduction using POD on both the registered snapshots matrix and unregistered snapshots matrix, the singular values decay is shown in Figure 1.8a with sharp decay for registered snapshots. Furthermore, in Figure 1.8b, the POD modes obtained via registration capture the vortex structure accurately (first row - Figure 1.8b), whereas the unregistered fails to capture the structure of the vortex (second row - Figure 1.8b).

We utilize the first POD mode obtained via registration and as previously, we employ the POD-R strategy to construct ROM for this numerical experiment. To employ shifts in the online phase, again we consider linear interpolations to build parameter t_i -to-optimal- Δ_i mappings. As specified in the previous case in the online phase, we utilize the predicted optimal shifts alongside the ROM prediction, to revert the predicted snapshots to the correct physical frame. The predicted snapshots in the correct physical frame for three-time instances $t \in \{25, 45, 58.75\}$ from the test set are shown in Figure 1.9, with the corresponding original snapshot as ground truth and the absolute difference. The prediction error for both the training and test set parameters is presented in 1.10. The relative L_2 error of the predicted snapshots is plotted for each parameter, along with the mean relative L_2 error.

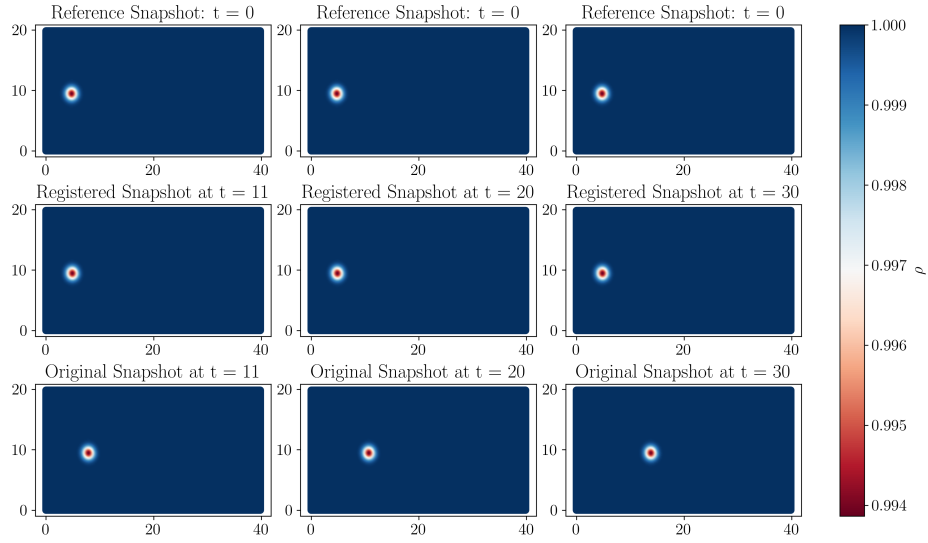


Fig. 1.7: Comparison of the isentropic convective vortex registered snapshots with the reference and the corresponding original snapshot.

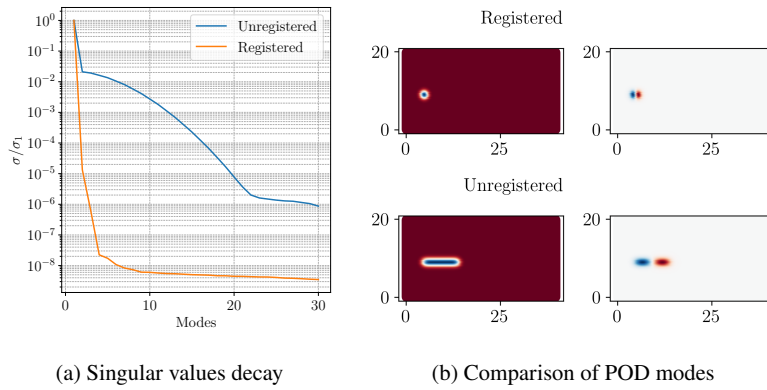


Fig. 1.8: **Left:** Comparison of singular values decay of registered snapshots matrix, labelled as Registered and of the unregistered snapshots matrix as Unregistered. **Right:** Showing the first two modes of the registered snapshots (first row - Registered) and showing the first two modes of the unregistered snapshots matrix (second row - Unregistered).

1.6 Conclusion

In this work, we employ model reduction for the transport-dominated problem via cross-correlation based snapshot registration. This cross-correlation based registra-

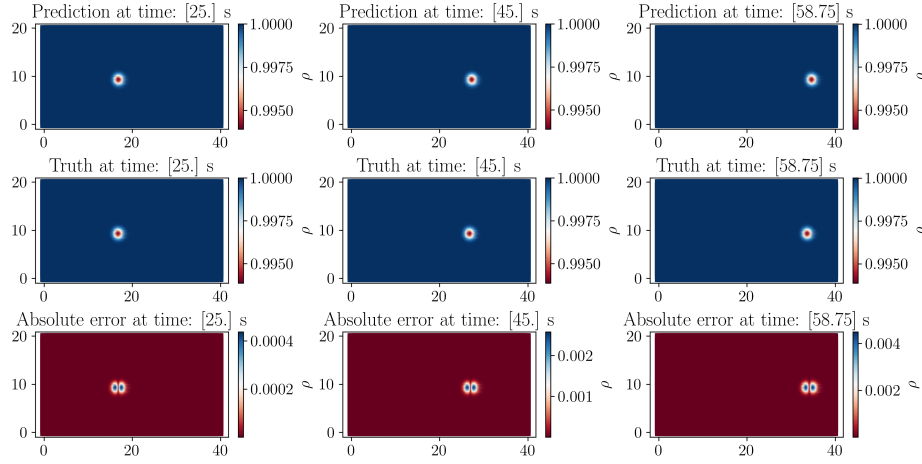


Fig. 1.9: Predictions of snapshots by ROM via cross-correlation based registrations of isentropic convective vortex test set parameters, showing for time instances $t \in \{25, 45, 58.75\}$ s.

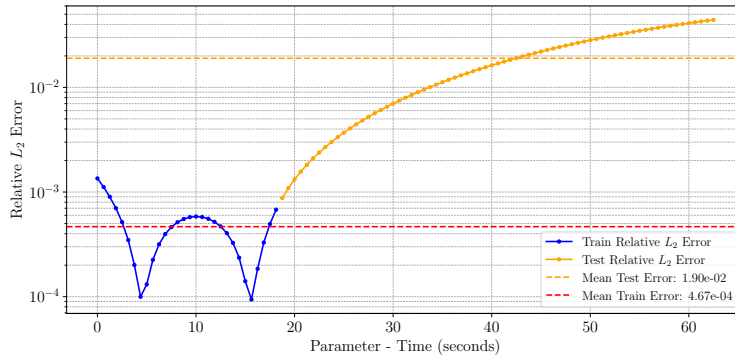


Fig. 1.10: Relative L_2 predictions error of the isentropic convective vortex ROM via cross-correlation based registrations, for both training and test set parameters.

tion accelerates the KnW decay and derives better linear approximation reduced subspace for the construction of efficient ROMs. We propose a complete framework consisting of offline-online stages for the construction of ROMs using the cross-correlation based snapshots registration. We tested our proposed workflow on transport-dominated problems: 1D travelling waves, and 2D isentropic vortex. In both numerical experiments, the proposed approach results in efficient and accurate ROMs. Nonetheless, the applicability of this approach is confined to certain transport-dominated problems where the structures of the transported features remain consistent. This approach is unsuitable for addressing advection-diffusion

problems. For our future work, we will investigate the approach by applying it to a vortex-shedding test case and address its effectiveness.

Acknowledgements

We acknowledge the PhD grant supported by industrial partner Danieli & C. S.p.A. and Programma Operativo Nazionale Ricerca e Innovazione 2014-2020, P.I. Gianluigi Rozza. GS acknowledges the financial support under the National Recovery and Resilience Plan (NRRP), Mission 4, Component 2, Investment 1.1, Call for tender No. 1409 published on 14.9.2022 by the Italian Ministry of University and Research (MUR), funded by the European Union – NextGenerationEU– Project Title ROMEU – CUP P2022FEZS3 - Grant Assignment Decree No. 1379 adopted on 01/09/2023 by the Italian Ministry of Ministry of University and Research (MUR).

References

- [1] J. Barnett and C. Farhat. Quadratic approximation manifold for mitigating the Kolmogorov barrier in nonlinear projection-based model order reduction. *Journal of Computational Physics*, 464:111348, Sept. 2022. ISSN 0021-9991. doi: 10.1016/j.jcp.2022.111348. URL <http://dx.doi.org/10.1016/j.jcp.2022.111348>.
- [2] K. Berberidis and I. Karybali. A new efficient cross-correlation based image registration technique with improved performance. In *2002 11th European Signal Processing Conference*, pages 1–4. IEEE, 2002.
- [3] J. Bruna, B. Peherstorfer, and E. Vanden-Eijnden. Neural Galerkin schemes with active learning for high-dimensional evolution equations. *Journal of Computational Physics*, 496:112588, Jan. 2024. ISSN 0021-9991. doi: 10.1016/j.jcp.2023.112588. URL <http://dx.doi.org/10.1016/j.jcp.2023.112588>.
- [4] N. Cagniard, R. Crisovan, Y. Maday, and R. Abgrall. Model Order Reduction for Hyperbolic Problems: a new framework. *HAL archive*, 2017. URL <https://hal.science/hal-01583224>.
- [5] S. Chelbi and A. Mekhmoukh. Features based image registration using cross correlation and radon transform. *Alexandria engineering journal*, 57(4):2313–2318, 2018.
- [6] F. Chinesta, A. Huerta, G. Rozza, and K. Willcox. Model reduction methods. *Encyclopedia of Computational Mechanics Second Edition*, page 1–36, Dec. 2017. doi: 10.1002/9781119176817.ecm2110. URL <http://dx.doi.org/10.1002/9781119176817.ecm2110>.
- [7] R. Crisovan, D. Torlo, R. Abgrall, and S. Tokareva. Model order reduction for parametrized nonlinear hyperbolic problems as an application to uncer-

- tainty quantification. *Journal of Computational and Applied Mathematics*, 348:466–489, March 2019. ISSN 0377-0427. doi: 10.1016/j.cam.2018.09.018. URL <http://dx.doi.org/10.1016/j.cam.2018.09.018>.
- [8] G. Debojyoti, L. John, and Y. Kim. HyPar 1.0 - Finite-Difference Hyperbolic-Parabolic PDE Solver on Cartesian Grids. <https://github.com/debog/hypar>. URL <https://hypar.github.io/index.html>.
- [9] N. Demo, M. Tezzele, and G. Rozza. EZyRB: Easy Reduced Basis method. "https://github.com/mathLab/EZyRB", April 2018. ISSN 2475-9066. URL <http://dx.doi.org/10.21105/joss.00661>.
- [10] C. Eckart and G. Young. The approximation of one matrix by another of lower rank. *Psychometrika*, 1(3):211–218, Sept. 1936. ISSN 1860-0980. doi: 10.1007/bf02288367. URL <http://dx.doi.org/10.1007/BF02288367>.
- [11] S. Fresca, L. Dede', and A. Manzoni. A Comprehensive Deep Learning-Based Approach to Reduced Order Modeling of Nonlinear Time-Dependent Parametrized PDEs. *Journal of Scientific Computing*, 87(2), April 2021. ISSN 1573-7691. doi: 10.1007/s10915-021-01462-7. URL <http://dx.doi.org/10.1007/s10915-021-01462-7>.
- [12] R. Geelen, S. Wright, and K. Willcox. Operator inference for non-intrusive model reduction with quadratic manifolds. *Computer Methods in Applied Mechanics and Engineering*, 403:115717, Jan. 2023. ISSN 0045-7825. doi: 10.1016/j.cma.2022.115717. URL <http://dx.doi.org/10.1016/j.cma.2022.115717>.
- [13] S. Gottlieb, C.-W. Shu, and E. Tadmor. Strong Stability-Preserving High-Order Time Discretization Methods. *SIAM Review*, 43(1):89–112, Jan. 2001. ISSN 1095-7200. doi: 10.1137/s003614450036757x. URL <http://dx.doi.org/10.1137/S003614450036757X>.
- [14] B. Haasdonk and M. Ohlberger. Adaptive basis enrichment for the reduced basis method applied to finite volume schemes. In *Proceedings of the 5th International Symposium on Finite Volumes for Complex Applications*, pages 471–478, 2008.
- [15] D. Hartman and L. K. Mestha. A deep learning framework for model reduction of dynamical systems. In *2017 IEEE Conference on Control Technology and Applications (CCTA)*. IEEE, Aug. 2017. doi: 10.1109/ccta.2017.8062736. URL <http://dx.doi.org/10.1109/CCTA.2017.8062736>.
- [16] J. S. Hesthaven, G. Rozza, and B. Stamm. *Certified Reduced Basis Methods for Parametrized Partial Differential Equations*. Springer International Publishing, 2016. ISBN 9783319224701. doi: 10.1007/978-3-319-22470-1. URL <http://dx.doi.org/10.1007/978-3-319-22470-1>.
- [17] C. Hoang, K. Chowdhary, K. Lee, and J. Ray. Projection-based model reduction of dynamical systems using space–time subspace and machine learning. *Computer Methods in Applied Mechanics and Engineering*, 389: 114341, Feb. 2022. ISSN 0045-7825. doi: 10.1016/j.cma.2021.114341. URL <http://dx.doi.org/10.1016/j.cma.2021.114341>.

- [18] A. Iollo and D. Lombardi. Advection modes by optimal mass transfer. *Physical Review E*, 89(2), Feb. 2014. ISSN 1550-2376. doi: 10.1103/physreve.89.022923. URL <http://dx.doi.org/10.1103/PhysRevE.89.022923>.
- [19] S. Jain, P. Tiso, J. B. Rutzmoser, and D. J. Rixen. A quadratic manifold for model order reduction of nonlinear structural dynamics. *Computers & Structures*, 188: 80–94, Aug. 2017. ISSN 0045-7949. doi: 10.1016/j.compstruc.2017.04.005. URL <http://dx.doi.org/10.1016/j.compstruc.2017.04.005>.
- [20] K. Kashima. Nonlinear model reduction by deep autoencoder of noise response data. In *2016 IEEE 55th Conference on Decision and Control (CDC)*. IEEE, Dec. 2016. doi: 10.1109/cdc.2016.7799153. URL <http://dx.doi.org/10.1109/CDC.2016.7799153>.
- [21] Y. Kim, Y. Choi, D. Widemann, and T. Zohdi. A fast and accurate physics-informed neural network reduced order model with shallow masked autoencoder. *Journal of Computational Physics*, 451:110841, Feb. 2022. ISSN 0021-9991. doi: 10.1016/j.jcp.2021.110841. URL <http://dx.doi.org/10.1016/j.jcp.2021.110841>.
- [22] K. Lee and K. T. Carlberg. Model reduction of dynamical systems on nonlinear manifolds using deep convolutional autoencoders. *Journal of Computational Physics*, 404:108973, March 2020. ISSN 0021-9991. doi: 10.1016/j.jcp.2019.108973. URL <http://dx.doi.org/10.1016/j.jcp.2019.108973>.
- [23] R. Mojjani and M. Balajewicz. Lagrangian basis method for dimensionality reduction of convection dominated nonlinear flows. *ArXiv*, abs/1701.04343, 2017. URL <https://api.semanticscholar.org/CorpusID:119505364>.
- [24] R. Mojjani and M. Balajewicz. Arbitrary Lagrangian Eulerian framework for efficient projection-based reduction of convection dominated nonlinear flows. In *APS Division of Fluid Dynamics Meeting Abstracts*, pages M1–008, 2017.
- [25] M. Nonino, F. Ballarin, G. Rozza, and Y. Maday. A reduced basis method by means of transport maps for a fluid–structure interaction problem with slowly decaying kolmogorov n -width. *Advances in Computational Science and Engineering*, 1(1):36–58, 2023. ISSN 2837-1739. doi: 10.3934/acse.2023002. URL <http://dx.doi.org/10.3934/acse.2023002>.
- [26] M. Ohlberger and S. Rave. Nonlinear reduced basis approximation of parameterized evolution equations via the method of freezing. *Comptes Rendus. Mathématique*, 351(23–24):901–906, Nov. 2013. ISSN 1778-3569. doi: 10.1016/j.crma.2013.10.028. URL <http://dx.doi.org/10.1016/j.crma.2013.10.028>.
- [27] B. Peherstorfer. Model Reduction for Transport-Dominated Problems via Online Adaptive Bases and Adaptive Sampling. *SIAM Journal on Scientific Computing*, 42(5):A2803–A2836, Jan. 2020. ISSN 1095-7197. doi: 10.1137/19m1257275. URL <http://dx.doi.org/10.1137/19M1257275>.
- [28] B. Peherstorfer. Breaking the Kolmogorov Barrier with Nonlinear Model Reduction. *Notices of the American Mathematical Society*, 69(05):1, May 2022. ISSN 1088-9477. doi: 10.1090/noti2475. URL <http://dx.doi.org/10.1090/noti2475>.

- [29] B. Peherstorfer and K. Willcox. Online Adaptive Model Reduction for Nonlinear Systems via Low-Rank Updates. *SIAM Journal on Scientific Computing*, 37(4):A2123–A2150, Jan. 2015. ISSN 1095-7197. doi: 10.1137/140989169. URL <http://dx.doi.org/10.1137/140989169>.
- [30] A. Pinkus. *n-Widths in Approximation Theory*. Springer Berlin Heidelberg, 1985. ISBN 9783642698941. doi: 10.1007/978-3-642-69894-1. URL <http://dx.doi.org/10.1007/978-3-642-69894-1>.
- [31] A. Quarteroni, A. Manzoni, and F. Negri. *Reduced Basis Methods for Partial Differential Equations*. Springer International Publishing, 2016. ISBN 9783319154312. doi: 10.1007/978-3-319-15431-2. URL <http://dx.doi.org/10.1007/978-3-319-15431-2>.
- [32] D. Rim, S. Moe, and R. J. LeVeque. Transport Reversal for Model Reduction of Hyperbolic Partial Differential Equations. *SIAM/ASA Journal on Uncertainty Quantification*, 6(1):118–150, Jan. 2018. ISSN 2166-2525. doi: 10.1137/17m1113679. URL <http://dx.doi.org/10.1137/17M1113679>.
- [33] F. Romor, G. Stabile, and G. Rozza. Non-linear Manifold Reduced-Order Models with Convolutional Autoencoders and Reduced Over-Collocation Method. *Journal of Scientific Computing*, 94(3), Feb. 2023. ISSN 1573-7691. doi: 10.1007/s10915-023-02128-2. URL <http://dx.doi.org/10.1007/s10915-023-02128-2>.
- [34] G. Rozza, G. Stabile, and F. Ballarin. *Advanced Reduced Order Methods and Applications in Computational Fluid Dynamics*. Society for Industrial and Applied Mathematics, Jan 2022. ISBN 9781611977257. doi: 10.1137/1.9781611977257. URL <http://dx.doi.org/10.1137/1.9781611977257>.
- [35] C.-W. Shu. *Essentially non-oscillatory and weighted essentially non-oscillatory schemes for hyperbolic conservation laws*, page 325–432. Springer Berlin Heidelberg, 1998. ISBN 9783540498049. doi: 10.1007/bfb0096355. URL <http://dx.doi.org/10.1007/BFb0096355>.
- [36] S. C. Spiegel, H. Huynh, and J. R. DeBonis. A survey of the isentropic euler vortex problem using high-order methods. In *22nd AIAA Computational Fluid Dynamics Conference*. American Institute of Aeronautics and Astronautics, June 2015. doi: 10.2514/6.2015-2444. URL <http://dx.doi.org/10.2514/6.2015-2444>.
- [37] G. Stabile and G. Rozza. Finite volume pod-galerkin stabilised reduced order methods for the parametrised incompressible navier–stokes equations. *Computers & Fluids*, 173:273–284, Sept. 2018. ISSN 0045-7930. doi: 10.1016/j.compfluid.2018.01.035. URL <http://dx.doi.org/10.1016/j.compfluid.2018.01.035>.
- [38] G. Stabile, F. Ballarin, G. Zuccarino, and G. Rozza. A reduced order variational multiscale approach for turbulent flows. *Advances in Computational Mathematics*, 45(5–6):2349–2368, June 2019. ISSN 1572-9044. doi: 10.1007/s10444-019-09712-x. URL <http://dx.doi.org/10.1007/s10444-019-09712-x>.

- [39] G. W. Stewart. On the Early History of the Singular Value Decomposition. *SIAM Review*, 35(4):551–566, Dec 1993. ISSN 1095-7200. doi: 10.1137/1035134. URL <http://dx.doi.org/10.1137/1035134>.
- [40] T. Taddei. A Registration Method for Model Order Reduction: Data Compression and Geometry Reduction. *SIAM Journal on Scientific Computing*, 42(2): A997–A1027, Jan. 2020. ISSN 1095-7197. doi: 10.1137/19m1271270. URL <http://dx.doi.org/10.1137/19M1271270>.
- [41] M. Tezzele, N. Demo, G. Stabile, and G. Rozza. *Chapter 9: Nonintrusive Data-Driven Reduced Order Models in Computational Fluid Dynamics*, page 203–222. Society for Industrial and Applied Mathematics, Jan. 2022. ISBN 9781611977257. doi: 10.1137/1.9781611977257.ch9. URL <http://dx.doi.org/10.1137/1.9781611977257.ch9>.
- [42] D. Torlo. Model Reduction for Advection Dominated Hyperbolic Problems in an ALE Framework: Offline and Online Phases. *arXiv preprint*, March 2020. doi: 10.48550/arxiv.2003.13735. URL <https://arxiv.org/abs/2003.13735>.
- [43] Z. Wang, K. Fidkowski, R. Abgrall, F. Bassi, D. Caraeni, A. Cary, H. Deconinck, R. Hartmann, K. Hillewaert, H. Huynh, N. Kroll, G. May, P. Persson, B. van Leer, and M. Visbal. High-order cfd methods: current status and perspective. *International Journal for Numerical Methods in Fluids*, 72(8):811–845, Jan. 2013. ISSN 1097-0363. doi: 10.1002/fld.3767. URL <http://dx.doi.org/10.1002/fld.3767>.
- [44] K. Washabaugh, D. Amsallem, M. Zahr, and C. Farhat. Nonlinear Model Reduction for CFD Problems Using Local Reduced-Order Bases. In *42nd AIAA Fluid Dynamics Conference and Exhibit*. American Institute of Aeronautics and Astronautics, June 2012. doi: 10.2514/6.2012-2686. URL <http://dx.doi.org/10.2514/6.2012-2686>.
- [45] Y.-T. Zhang and C.-W. Shu. ENO and WENO Schemes . In *Handbook of Numerical Methods for Hyperbolic Problems - Basic and Fundamental Issues*, page 103–122. Elsevier, 2016. doi: 10.1016/bs.hna.2016.09.009. URL <http://dx.doi.org/10.1016/bs.hna.2016.09.009>.